Letter

Primary quantum thermometry of mm-wave blackbody radiation via induced state transfer in Rydberg states of cold atoms

Noah Schlossberger,[1,*] Andrew P. Rotunno,[1] Stephen P. Eckel,[2] Eric B. Norrgard,[2] Dixith Manchaiah,[3,4] Nikunjkumar Prajapati,[1] Alexandra B. Artusio-Glimpse,[1] Samuel Berweger,[1] Matthew T. Simons,[1] Dangka Shylla,[3,4] William J. Watterson,[3,4] Charles Patrick,[3,4] Adil Meraki,[3,4] Rajavardhan Talashila,[3,5] Amanda Younes,[6] David S. La Mantia,[2] and Christopher L. Holloway[1]

[1]*National Institute of Standards and Technology, Boulder, Colorado 80305, USA*

[2]*National Institute of Standards and Technology, Gaithersburg, Maryland 20899, USA*

[3]*Associate of the National Institute of Standards and Technology, Boulder, Colorado 80305, USA*

[4]*Department of Physics, University of Colorado, Boulder, Colorado 80309, USA*

[5]*Department of Electrical Engineering, University of Colorado, Boulder, Colorado 80309, USA*

[6]*Department of Physics and Astronomy, University of California, Los Angeles, California 90095, USA*

(Received 16 October 2024; accepted 7 December 2024; published 23 January 2025)

Rydberg states of alkali-metal atoms are highly sensitive to electromagnetic radiation in the GHz-to-THz regime because their transitions have large electric dipole moments. Consequently, environmental blackbody radiation (BBR) can couple Rydberg states together at μs timescales. Here, we track the BBR-induced transfer of a prepared Rydberg state to its neighbors and use the evolution of these state populations to characterize the BBR field at the relevant wavelengths, primarily at 130 GHz. We use selective field ionization readout of Rydberg states with principal quantum number $n \sim 30$ in ^{85}Rb and substantiate our ionization signal with a theoretical model. With this detection method, we measure the associated blackbody-radiation-induced time dynamics of these states, reproduce the results with a simple semiclassical population transfer model, and demonstrate that this measurement is temperature sensitive with a statistical sensitivity to the fractional temperature uncertainty of 0.09 $\mathrm{Hz}^{-1/2}$, corresponding to 26 K $\mathrm{Hz}^{-1/2}$ at room temperature. This represents a calibration-free SI-traceable temperature measurement, for which we calculate a systematic fractional temperature uncertainty of 0.006, corresponding to 2 K at room temperature when used as a primary temperature standard.

DOI: 10.1103/PhysRevResearch.7.L012020

Radiation thermometry is used widely in science and engineering, including in remote sensing, weather prediction, and manufacturing, among others. Typical classical radiation thermometers require calibration, mostly using the classic blackbody cavity, which emits a known amount of radiation given its temperature through Planck's law. This arduous calibration process not only requires calibrating the radiation thermometers but also the blackbody itself and the contact thermometers used to measure the blackbody's temperature. As such, the calibration is subject to offsets and errors [1]. However, the redefinition of the SI in 2019 has opened new opportunities for calibration-free radiation thermometers that directly realize the kelvin. Here, we demonstrate such a quantum-based thermometer based on blackbody radiation-induced transitions within Rydberg atoms.

Rydberg states of alkali-metal atoms have been used as electric field sensors in a comprehensive set of application spaces because their large transition dipole moments make them sensitive to radiation in the GHz-to-THz range [2–5]. Likewise, Rydberg atoms are also sensitive to blackbody radiation (BBR) at those same frequencies. Blackbody radiation has three predominant effects on Rydberg atoms [6,7]. First, it induces a common AC Stark shift amongst the Rydberg levels, first measured by Hollberg and Hall [8]. This shift, roughly 2.4 kHz at room temperature, has been proposed as a potential thermometer for optical clocks [9]; currently the ambient BBR represents the largest contribution to an optical clock's uncertainty budget [10,11] and is quantified using contact thermometers and models of the surrounding environment's emissivity [11]. Second and third, blackbody radiation induces ionization [12,13] and transitions between different Rydberg states [14–16]. Reference [17] found that the relative statistical temperature sensitivity σ_T/T can approach $1/\sqrt{N_{\mathrm{Ryd}}}$, where N_{Ryd} is the number of Rydberg atoms, by measuring any of the above three effects.

Recently, we realized a radiation thermometer based on monitoring fluorescence from BBR-populated states in an optically excited vapor cell with a statistical uncertainty as low as $\sigma_T/T = 4 \times 10^{-4}$ [18]. It operated near the peak of the blackbody spectrum by monitoring optical fluorescence induced by BBR excitation at 24.6 THz. In the microwave regime, we reinterpreted the state population data of Ref. [16]

*Contact author: noah.schlossberger@nist.gov

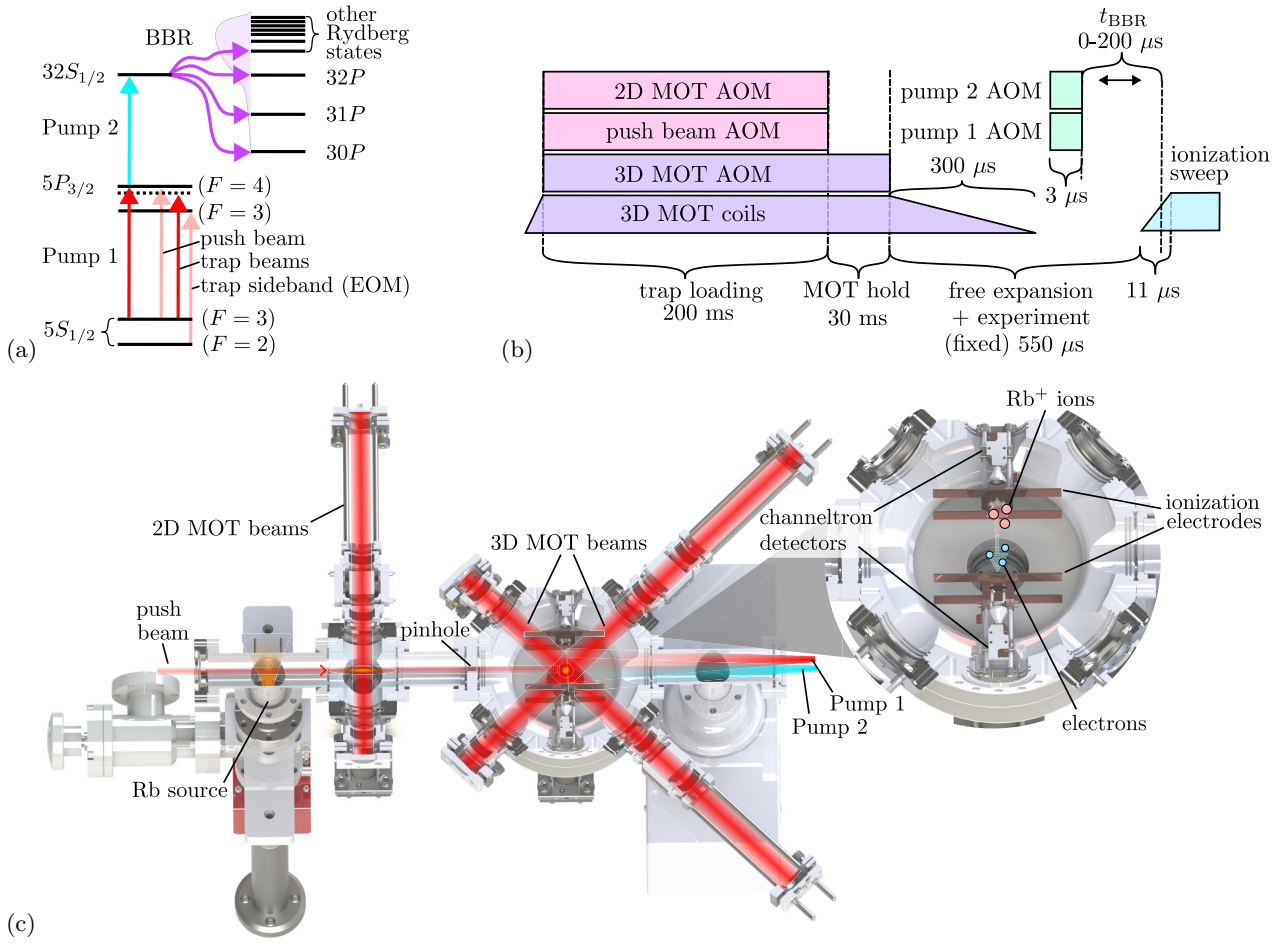

FIG. 1. The experimental scheme for measuring BBR-induced state transfer. (a) Energy level diagram of the experiment. (b) Timing sequence of the experiment. (c) Physical layout of the experiment. Not shown is a retroreflected vertical beam in each of the 2D and 3D MOTs and the anti-Helmholtz coils of the 3D MOT, which are aligned vertically (out of the page).

taken by state selective field ionization (SFI) to derive the radiometric temperature around the frequency of 167 GHz with an overall statistical uncertainty of about 2% [5].

The radiation thermometer described here is conceptually similar to the proof-of-principle demonstrated in Refs. [5,16], while being optimized for radiometric thermometry and using cold atoms to suppress collisional systematics. We realize the kelvin by tracking the BBR-induced transfer from the $32S$ state of ^{85}Rb to its neighboring states, particularly to the $32P$ state. This transition is sensitive to BBR radiation at a frequency of 130 GHz. Such microwave frequencies have posed a unique challenge in radiometry, as the BBR energy density is roughly 2000 times lower than the peak around 30 THz at 300 K. The transition rate between $32S$ and $32P$ is essentially the product of the BBR energy density, the transition dipole moments, and SI constants, meaning they represent an SI-traceable primary temperature measurement [17].

The measurement scheme relies on several well-developed techniques [16,19,20] and is as follows: We prepare a sample of roughly 10^6 ^{85}Rb atoms at roughly 1 mK in a magneto-optical trap (MOT). We then pulse a two-photon excitation to a Rydberg state. We wait a time of $t_{\mathrm{BBR}} < 100$ μs for blackbody radiation to couple from this Rydberg state to other states. Next, we sweep an electric field to selectively ionize Rydberg state atoms [21] and collect the ions and stripped electrons using electron avalanche detectors. Each measurement takes a time τ_{shot} of 354 ms, consisting of 231 ms of experiment [Fig. 1(b)] and 123 ms of dead time.

Figure 1 details the relevant energy level diagram (a), the timing (b), and the physical layout (c) of the experiment. We heat a resistive dispenser of Bi_2Rb_3 alloy, which then releases pure Rb vapor. The vapor makes its way into a two-dimensional (2D) MOT, consisting of two retroreflected laser beams (−20 MHz detuned from the D_2 line ($5S_{1/2} \rightarrow 5P_{3/2}$) with ∼100 mW in a 1-cm 1-σ beam radius) and four permanent bar magnets. The atoms are collected here, and a weak push beam (resonant to the D_2 line with ∼100 μW in a 2-mm 1-σ beam radius) pushes the atoms through a 4-mm pinhole into a three-dimensional (3D) MOT. Loading from the 2D to the 3D MOT through a pinhole allows for the 3D MOT chamber to be free of background room-temperature atoms. The 2D MOT chamber is evacuated below 1.3×10^{-9} Pa, and the 3D MOT chamber is evacuated to 7.1×10^{-8} Pa.

The 3D MOT consists of three retroreflected laser beams (−20 MHz detuned from the D_2 line with ∼80 mW of power in a 1-cm 1-σ beam radius) and two coils in an anti-Helmholtz configuration. The current through the coils is controlled with an insulated-gate bipolar transistor which allows the field

to be switched off in ∼300 μs. We estimate the cloud to contain $\sim 2 \times 10^6$ atoms, of which ∼5400 participate in the measurement, with a temperature of ∼0.5 mK (details in the Supplemental Material [25]).

After the trap is released, the atoms are excited to a Rydberg state via Pump 1 (resonant to the D_2 line with ∼9mW in a 5-mm 1-σ beam radius) and Pump 2 (resonant on the $5P_{3/2} \rightarrow 32S_{1/2}$ transition with 57 mW in a 5 mm 1-σ beam radius, locked to a two-photon electromagnetically induced transparency in a reference cell). After the blackbody coupling time t_{BBR}, ionization is performed with two electrodes placed 56 mm apart that are swept from 0 to 3 kV in ∼7 μs, and the ions and their electrons are collected using channel electron multiplier (CEM), or "channeltron," detectors.

The current incident on the anode of the CEM is converted into a voltage using a transimpedance amplifier with a gain of 10^3 V/A and recorded on an oscilloscope. The circuit driving the ionization electrodes is diagramed in the Supplemental Material [25]. The initial state of $32S_{1/2}$ is chosen for experimental reasons. Generally, lower n states are more resolvable with SFI, but require a larger electric field to ionize. An initial Rydberg state of $32S_{1/2}$ is chosen because it is the lowest state that ionizes optimally given the timing constraints of the experiment.

To make sense of the resulting SFI signal, we use a theoretical model [21,22]. Our model first computes the eigenenergies and eigenstates using a sufficiently large basis for all relevant electric fields during the ramp. We then evolve the initial state through this Stark map according to the Schrödinger equation using the correct electric field ramp with time. This properly accounts for both adiabatic and diabatic transitions. At each point in the sweep, a Stark eigenstate will be ionized if its classical ionization field $E_{\mathrm{ionization}}$ is reached, calculated as [23]

$$E_{\mathrm{ionization}} = \frac{m_e a_0}{4e\hbar^2} U_i^2, \tag{1}$$

where U_i is the energy of the state below the free electron continuum, m_e is the mass of the electron, a_0 is the Bohr radius, and $\hbar$ is the reduced Planck constant. Each Stark eigenstate will contribute to the SFI signal when its ionization energy is reached, with a relative amplitude corresponding to the likelihood of arriving in that Stark eigenstate given the initial state. Such a calculation for $32S_{1/2}$ is shown in Fig. 2(a).

Both the ions and the electrons produced by the electric field ramp are collected. The ion signal is considerably stronger than the electron signal, and the electron signal requires capacitive readout which limits the detection bandwidth. However, the electrons arrive near instantaneously, while the ions' mass places their transit time at timescales of order of the length of the ionization ramp. Therefore, we use the electron signal with a well-defined applied field to time relationship to identify peaks, and we use the ion signal to count state populations.

The field at which ionization occurs is calculated from the electron time-of-arrival by recording the voltages applied to each electrode with a high-voltage probe and using a finite element simulation of the experiment to convert voltages at the electrodes to fields at the center of the trap (details in the Supplemental Material [25]). The electron signal traces over

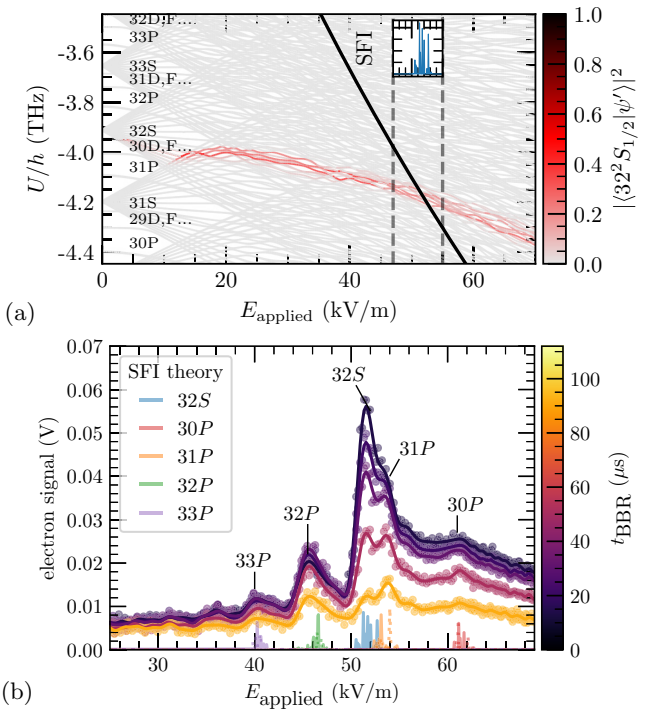

FIG. 2. Theoretical model of SFI. (a) The Stark map is calculated for a ramp from 0 to 70 kV/m in 11 μs, and for each point in the ramp the overlap of each state with the original state $32S_{1/2}$ is shown in the colormap. The ionization energy is drawn as a solid black line, and the resulting expected SFI signal is shown in an inset. (b) An equivalent calculation is performed for each relevant state, and the measured electron ionization signal at various t_{BBR} is overlayed. For the P state theory, solid lines indicate $P_{3/2}$ state contributions while dotted lines represent $P_{1/2}$ state contributions.

a span of 100 μs of BBR-induced coupling after populating $32S$ is shown in Fig. 2(b). Overlayed are the theoretical SFI contributions from the relevant states, each calculated as in Fig. 2(a). Agreement between the theoretical fields at which ionization occurs and the measured ionization signal demonstrates adequate understanding of the field ionization process and confidently identifies each detected peak.

The population in each state can be counted by integrating each peak on the ion signal, which has sufficient bandwidth to fully separate each peak [Fig. 3(a)]. The saturation and the kinetic energy-dependent gain of the detector are characterized in the Supplemental Material [25] and corrections are applied before integrating the signal to count ions. The ion signal at various blackbody evolution times t_{BBR} is shown in Fig. 3(b). Initially, the $32S$ state is populated by the pump lasers. Blackbody radiation then couples population from $32S$ to nearby Rydberg states that are dipole-allowed transitions, and eventually all population decays to states not accessible via SFI readout.

A theoretical model for the BBR-induced state transfer can be constructed analytically [16]. Because natural decay and blackbody-driven couplings are both incoherent processes, we can model the time dynamics of the system using a semiclassical rate equation model. If the transfer rate from a state $|i\rangle$ to a state $|j\rangle$ induced by blackbody radiation and natural decay

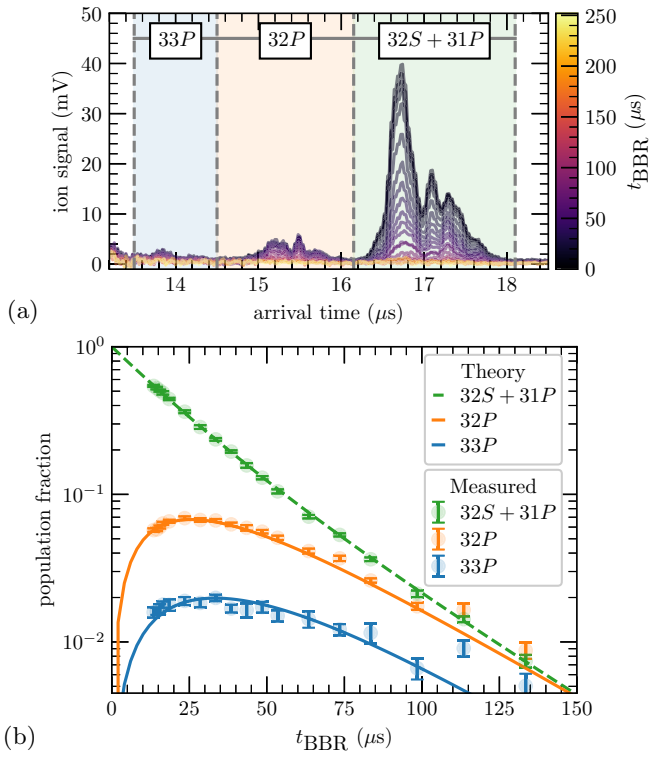

FIG. 3. Population tracking of the ionized states as a function of the BBR evolution time t_{BBR} in a room-temperature (296 K) environment. (a) Time dynamics of the ion signal, with each peak labeled with the corresponding quantum state. (b) Each peak is integrated to count the atom population in each state. Each data point represents 40 measurements. The solid lines represent theoretical time dynamics from Eq. (3).

is given by $\Gamma_{i\to j}$ and the lifetime of a state $|i\rangle$ from all such couplings is τ_i. Then for a set of N states with populations n_i the time dynamics are given by

$$\frac{\partial}{\partial t}\begin{bmatrix} n_1 \\ n_2 \\ \dots \\ n_N \end{bmatrix} = \underbrace{\begin{bmatrix} -1/\tau_1 & \Gamma_{2\to1} & \dots & \Gamma_{N\to1} \\ \Gamma_{1\to2} & -1/\tau_2 & \dots & \Gamma_{N\to2} \\ \dots & \dots & \dots & \dots \\ \Gamma_{1\to N} & \Gamma_{2\to N} & \dots & -1/\tau_N \end{bmatrix}}_{\equiv M} \begin{bmatrix} n_1 \\ n_2 \\ \dots \\ n_N \end{bmatrix}, \quad (2)$$

where the off-diagonal matrix elements represent individual couplings and the diagonal matrix elements represent all transfer out of a state. This differential equation has the solution

$$\begin{bmatrix} n_1(t) \\ n_2(t) \\ \dots \\ n_N(t) \end{bmatrix} = e^{Mt} \begin{bmatrix} n_1(t=0) \\ n_2(t=0) \\ \dots \\ n_N(t=0) \end{bmatrix}. \quad (3)$$

States with principal quantum numbers from $n = 5$ through $n = 50$ and angular momentum quantum numbers $\ell = 0$ through $\ell = 20$ are considered, with the initial state taken to be that with only $|32S\rangle$ populated. The BBR and decay-induced transition rates $\Gamma_{i\to j}$ and lifetimes τ_i contained in the matrix M are calculated using the ARC PYTHON package [24]. Assuming that only the $|32S_{1/2}\rangle$ state is initially populated, the solution at room temperature is compared with measurement in Fig. 3(b). Note that Rydberg $P_{1/2}$ and $P_{3/2}$ states are included separately in the model, and the "P state" populations are taken to be the sum of these two. Agreement with the theoretical time dynamics predicted by Eq. (3) is achieved with an overall normalization as well as allowing an offset in t_{BBR} due to finite optical pumping and ionization ramp times.

To turn state population dynamics into a primary BBR temperature measurement, it is necessary to make a direct comparison of measured values to theory, without the need for scaling factors. One way to parametrize the time dynamics in a dimensionless way is with the ratio $\mathcal{R}$ of the populations in the two measured peaks:

$$\mathcal{R} \equiv \frac{N_{|32P\rangle}}{N_{|32S\rangle} + N_{|31P\rangle}}. \quad (4)$$

The value of $\mathcal{R}$ at any time is approximately linearly proportional to the environmental temperature, as at higher temperatures there is a higher BBR photon density to couple $32S$ to $32P$. This ratio is a temperature-sensitive metric that is independent of fluctuations in the trap loading and in the preparation efficiency of the initial Rydberg state.

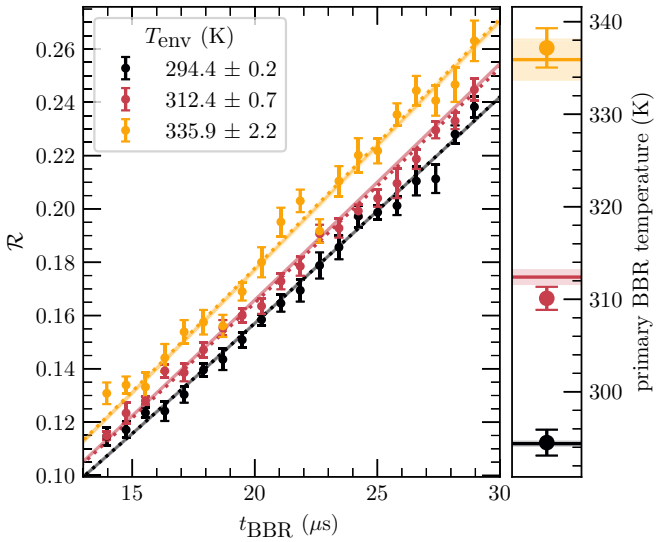

RTD temps. (K)	T_{env} (K)	BBR temp. (K)
294, 294, 295, 294	294.4 ± 0.2	294.5 ± 1.4
312, 313, 314, 310	312.4 ± 0.7	310.1 ± 1.3
337, 336, 341, 329	335.9 ± 2.2	337.2 ± 2.1

FIG. 4. Demonstration of primary thermometry as the vacuum chamber is heated to various temperatures. Left: The peak ratio $\mathcal{R}$ as a function of blackbody evolution time t_{BBR}. Points with error bars are measured values with each point representing 40 measurements. Solid lines indicate theoretical predictions using Eq. (3) and the classically measured temperature T_{env}, with a shaded region representing the uncertainty of the classical measurement. Dotted lines represent temperature-floated fits based on Eq. (3) that are used to determine the primary BBR temperature measurement. Right: The result of the temperature fits. Each primary temperature measurement is represented as a point with errorbars associated to the statistical uncertainty of the fit. The solid lines represent the associated classically measured T_{env}.

TABLE I. Uncertainty budget for the temperature measurement.

Systematic uncertainty	σ_T/T
Detector nonlinearity	0.002
Ion time-of-flight overlap	0.005
Determination of $t_{\mathrm{BBR}} = 0$	0.002
Detection signal artifacts	0.003
Time-dependent gain calibration	1×10^{-5}
Total (quadrature sum)	0.006
Statistical senstivity	$\mathcal{S}(\sigma_T/T)$ ($\mathrm{Hz}^{-1/2}$)
Total	0.086 ± 0.009

To demonstrate the temperature sensitivity of this measurement, the vacuum chamber surrounding the 3D MOT is wrapped in multilayer aluminum foil and heated with a resistive element. The heaters are held at constant power for at least 8 h before each measurement to establish thermal equilibrium. The temperature of the environment is measured with resistance temperature detectors at four locations on the surface of the vacuum chamber, and the environmental temperature T_{env} is taken to be the mean of these measurements. We neglect the microwave reflectivity of the elements inside of the vacuum chamber because the system is in thermal equilibrium except for a small (<3%) solid angle provided by the viewports.

The resulting population ratios measured are shown in Fig. 4. Each trace of $\mathcal{R}$ is turned into a primary temperature measurement by fitting it to a theoretical value of $\mathcal{R}(t_{\mathrm{BBR}}, T)$ calculated from Eq. (3), with the temperature floated. The measurement is most sensitive in the first ∼20 μs of BBR evolution time because all relevant states are most populated in this period. Each trace in Fig. 4 represents a 4.7-min measurement which yields a mean of 1.6 K of statistical temperature uncertainty.

A summary of systematic and statistical uncertainties are provided in Table I, where σ_T/T is the fractional uncertainty of the measured temperature, and $\mathcal{S}(\sigma_T/T) \equiv \sigma_T/T\sqrt{\tau_{\mathrm{meas}}}$ is the statistical sensitivity. Here, τ_{meas} is the total measurement time including dead time. Detailed calculations for each systematic as well as the statistical sensitivity are included in the Supplemental Material [25]. We find that as a primary (calibration-free) temperature measurement, our system has a fractional systematic uncertainty of 0.006 representing 2 K of absolute temperature uncertainty at room temperature.

We have described a method for measuring blackbody radiation via tracking the population of Rydberg states in cold atoms. We have demonstrated selective field ionization to read out $n \sim 30$ states of ^{85}Rb and correlated these measurements to theoretical ionization fields. We used this readout scheme to measure BBR-induced state transfer and decay in Rydberg states, providing a semiclassical model for the time dynamics, and demonstrated that this measurement is temperature sensitive. We resolve 1.6 K in 4.7 min, with an absolute uncertainty of 2 K. This work represents a proof-of-concept for using Rydberg atoms as an SI-traceable radiation thermometer.

This work was funded by the National Institute of Standards and Technology (NIST) through the NIST-on-a-Chip (NOAC) and through the Innovations in Measurement Science (IMS) program.

The authors have no conflicts of interest to disclose.

Data availability. The data relevant to the findings of this work are available at Ref. [29].

[1] A. C. Carter, R. U. Datla, T. M. Jung, A. W. Smith, and J. A. Fedchak, Low-background temperature calibration of infrared blackbodies, Metrologia **43**, S46 (2006).

[2] H. Fan, S. Kumar, J. Sedlacek, H. Kübler, S. Karimkashi, and J. P. Shaffer, Atom based RF electric field sensing, J. Phys. B: At., Mol. Opt. Phys. **48**, 202001 (2015).

[3] J. A. Sedlacek, A. Schwettmann, H. Kübler, R. Löw, T. Pfau, and J. P. Shaffer, Microwave electrometry with Rydberg atoms in a vapour cell using bright atomic resonances, Nat. Phys. **8**, 819 (2012).

[4] A. Artusio-Glimpse, M. T. Simons, N. Prajapati, and C. L. Holloway, Modern RF measurements with hot atoms: A technology review of Rydberg atom-based radio frequency field sensors, IEEE Microwave Mag. **23**, 44 (2022).

[5] N. Schlossberger, Nikunjkumar Prajapati, S. Berweger, A. P. Rotunno, A. B. Artusio-Glimpse, M. T. Simons, A. A. Sheikh, E. B. Norrgard, S. P. Eckel, and C. L. Holloway, Rydberg states of alkali atoms in atomic vapour as Si-traceable field probes and communications receivers, Nat. Rev. Phys. **6**, 606 (2024)

[6] T. F. Gallagher and W. E. Cooke, Interactions of blackbody radiation with atoms, Phys. Rev. Lett. **42**, 835 (1979).

[7] J. W. Farley and W. H. Wing, Accurate calculation of dynamic Stark shifts and depopulation rates of Rydberg energy levels induced by blackbody radiation: Hydrogen, helium, and alkali-metal atoms, Phys. Rev. A **23**, 2397 (1981).

[8] L. Hollberg and J. L. Hall, Measurement of the shift of Rydberg energy levels induced by blackbody radiation, Phys. Rev. Lett. **53**, 230 (1984).

[9] V. D. Ovsiannikov, A. Derevianko, and K. Gibble, Rydberg spectroscopy in an optical lattice: Blackbody thermometry for atomic clocks, Phys. Rev. Lett. **107**, 093003 (2011).

[10] A. D. Ludlow, T. Zelevinsky, G. K. Campbell, S. Blatt, M. M. Boyd, M. H. G. de Miranda, M. J. Martin, J. W. Thomsen, S. M. Foreman, J. Ye, T. M. Fortier, J. E. Stalnaker, S. A. Diddams, Y. Le Coq, Z. W. Barber, N. Poli, N. D. Lemke, K. M. Beck, and C. W. Oates, Sr lattice clock at 1×10^{-16} fractional uncertainty by remote optical evaluation with a Ca clock, Science **319**, 1805 (2008).

[11] K. Beloy, N. Hinkley, N. B. Phillips, J. A. Sherman, M. Schioppo, J. Lehman, A. Feldman, L. M. Hanssen, C. W. Oates, and A. D. Ludlow, Atomic clock with 1×10^{-18} room-temperature blackbody stark uncertainty, Phys. Rev. Lett. **113**, 260801 (2014).

[12] W. P. Spencer, A. G. Vaidyanathan, D. Kleppner, and T. W. Ducas, Photoionization by blackbody radiation, Phys. Rev. A **26**, 1490 (1982).

[13] I. I. Beterov, D. B. Tretyakov, I. I. Ryabtsev, V. M. Entin, A. Ekers, and N. N. Bezuglov, Ionization of Rydberg atoms by blackbody radiation, New J. Phys. **11**, 013052 (2009).

[14] H. Figger, G. Leuchs, R. Straubinger, and H. Walther, A photon detector for submillimetre wavelengths using Rydberg atoms, Opt. Commun. **33**, 37 (1980).

[15] W. P. Spencer, A. G. Vaidyanathan, D. Kleppner, and T. W. Ducas, Temperature dependence of blackbody-radiation-induced transfer among highly excited states of sodium, Phys. Rev. A **25**, 380 (1982).

[16] E. J. Galvez, J. R. Lewis, B. Chaudhuri, J. J. Rasweiler, H. Latvakoski, F. De Zela, E. Massoni, and H. Castillo, Multistep transitions between Rydberg states of Na induced by blackbody radiation, Phys. Rev. A **51**, 4010 (1995).

[17] E. B. Norrgard, S. P. Eckel, C. L. Holloway, and E. L. Shirley, Quantum blackbody thermometry, New J. Phys. **23**, 033037 (2021).

[18] D. S. La Mantia, M. Lei, N. Prajapati, N. Schlossberger, M. T. Simons, C. L. Holloway, J. Scherschligt, S. P. Eckel, and E. B. Norrgard, Compact blackbody radiation atomic sensor: Measuring temperature using optically excited atoms in vapor cells, arXiv:2411.13426.

[19] T. Cantat-Moltrecht, R. Cortiñas, B. Ravon, P. Méhaignerie, S. Haroche, J. M. Raimond, M. Favier, M. Brune, and C. Sayrin, Long-lived circular Rydberg states of laser-cooled rubidium atoms in a cryostat, Phys. Rev. Res. **2**, 022032(R) (2020).

[20] M. Archimi, M. Ceccanti, M. Distefano, L. Di Virgilio, R. Franco, A. Greco, C. Simonelli, E. Arimondo, D. Ciampini, and O. Morsch, Measurements of blackbody-radiation-induced transition rates between high-lying S, P, and D Rydberg levels, Phys. Rev. A **105**, 063104 (2022).

[21] T. F. Gallagher, *Rydberg Atoms*, Cambridge Monographs on Atomic, Molecular and Chemical Physics (Cambridge University, Cambridge, England, 1994).

[22] V. C. Gregoric, J. J. Bennett, B. R. Gualtieri, A. Kannad, Z. C. Liu, Z. A. Rowley, T. J. Carroll, and M. W. Noel, Improving the state selectivity of field ionization with quantum control, Phys. Rev. A **98**, 063404 (2018).

[23] W. E. Cooke and T. F. Gallagher, Dependence of Rydberg-state field-ionization thresholds on $|m_l|$, Phys. Rev. A **17**, 1226 (1978).

[24] N. Šibalić, J. D. Pritchard, C. S. Adams, and K. J. Weatherill, ARC: An open-source library for calculating properties of alkali Rydberg atoms, Comput. Phys. Commun. **220**, 319 (2017).

[25] See Supplemental Material at http://link.aps.org/supplemental/10.1103/PhysRevResearch.7.L012020 for atom trap characterization, ionization methods, and detailed uncertainty analysis, which includes Refs. [26–28].

[26] S. Pradhan and B. N. Jagatap, Measurement of temperature of laser cooled atoms by one-dimensional expansion in a magneto-optical trap, Rev. Sci. Instrum. **79**, 013101 (2008).

[27] U. Volz and H. Schmoranzer, Precision lifetime measurements on alkali atoms and on helium by beam–gas–laser spectroscopy, Phys. Scr. **T65**, 48 (1996).

[28] D. Tong, S. M. Farooqi, J. Stanojevic, S. Krishnan, Y. P. Zhang, R. Côté, E. E. Eyler, and P. L. Gould, Local blockade of Rydberg excitation in an ultracold gas, Phys. Rev. Lett. **93**, 063001 (2004).

[29] doi:10.18434/mds2-3499.